2018 IEEE/RSJ International Conference on Intelligent Robots and Systems (IROS)
Madrid, Spain, October 1-5, 2018

Ceiling Effects for Surface Locomotion of Small Rotorcraft

Yi Hsuan Hsiao and Pakpong Chirarattananon†

***Abstract*— Motivated by the potential of bimodal aerial and surface locomotion as an energy saving strategy for small flying robots, we investigate the effects of a flat overhang surface in the vicinity of a spinning propeller. We employ the classical momentum theory and the blade element method to describe the "ceiling effects" in regards to the generated thrust, power, and rotational speed of the propeller in terms of a normalized distance between the ceiling and the propeller. Validating experiments were performed on a benchtop setup, and the results are in agreement with the proposed models. The presence of a ceiling was found to reduce the power consumption by more than a factor of three for the same thrust force. Overall, our findings show promise, paving the way for the use of perching maneuvers by small rotorcraft to extend their missions.**

I. Introduction

In recent years, there has been rapid development of small human-friendly aerial vehicles [1]. These flying machines, ranging from millimeter-scale flapping-wing robots [2], [3] to hybrid fixed-wing devices [4], [5], and a swarm of drones [6], [7], have immense potential applications related to services, agriculture, transportation, etc. Among various platforms of Micro Aerial Vehicles (MAVs), multirotor vehicles have attained remarkable popularity because of the simple mechanical designs and the wide range of functionalities.

One of the primary challenges encountered in the application of these multirotor systems is the high energetic consumption of flight. Particularly, as the vehicle size shrinks, the low Reynolds number leads to increased viscous losses [1]. The unfavorable scaling phenomenon severely affects the flight endurance. This acutely limits the capability of the robots, preventing the use of small MAVs for long-range missions or tasks that necessitate an extended operational time.

Recently, researchers have explored multimodal locomotion as a workaround solution to the energetic efficiency problem. The combination of aerial and surface locomotion has emerged, allowing robots to perch and attach to vertical surfaces or overhangs using various adhesion or mechanical attachment techniques [3], [8]–[11]. With the reduction in power consumption while perching, the robots continue to perform useful functions such as surveillance, inspection, and communication.

In this paper, we study the possibility of using the ceiling effects for small rotorcraft as a simple, energetically efficient approach for a robot to perch on an overhang. In the proximity of a ceiling, the robot experiences a substantial increase in the generated thrust, enabling the robot to stay aloft in the vicinity of a ceiling consuming significantly less power. The implementation of a lightweight structure on the airframe of the robot as shown in figure 1 would prevent the robot from directly colliding with the ceiling while it remains close to the surface, benefiting from the ceiling effects.

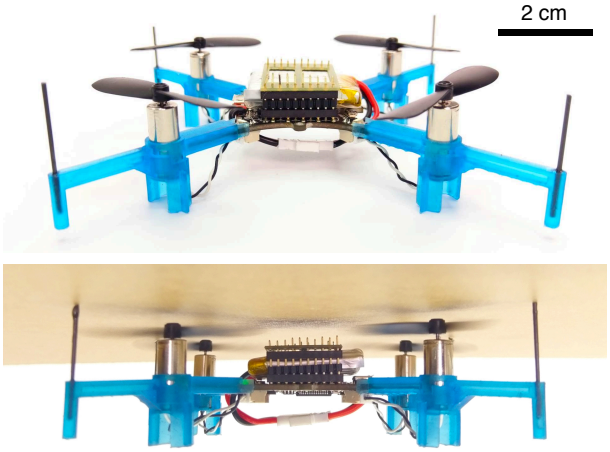

Fig. 1. (Top) A prototype made of a Crazyflie 2.0 Nano Quadcopter with a modified airframe. The robot, equipped with rigid poles for preventing a collision with the ceiling, weighs 31.7 g (compared to the original of 28.1 g). (Bottom) A photo of the robot perching on an overhang using the ceiling effects as a demonstration of the proposed concept.

To date, there has been limited research on the effects of a ceiling on a spinning propeller, whereas the aerodynamics of a rotorcraft in the proximity of the ground has previously been investigated for helicopters and small quadrotors based on the method of images and a surface singularity method [12]–[15]. The ground effect was found negligible when the rotor is one diameter off the ground [15], [16], rendering it practically ineffective for MAVs in regular flights. In contrast, we foresee that small rotorcraft can beneficially exploit the ceiling effect when operating indoor or under structural overhangs as the gap between the ceiling and the rotors is minimized. The novelty of this paper lies in the systematic study of the ceiling effects for potential hybrid aerial-surface locomotion for small multi-rotor robots.

To gain further insights into the ceiling effects, we offer a simple aerodynamics model to explain the observed proximity effects based on the momentum theory. The analysis shows how the ceiling effects reduce the power consumption of the propeller by a factor defined as a ceiling coefficient. The blade element method further provides the relationship between the thrust and the rotational speed of the propeller.

†The authors are with the Department of Mechanical and Biomedical Engineering, City University of Hong Kong, Hong Kong SAR, China (email: pakpong.c@cityu.edu.hk).

This work was partially supported by the Research Grants Council of the Hong Kong Special Administrative Region of China (grant number CityU-11215117).

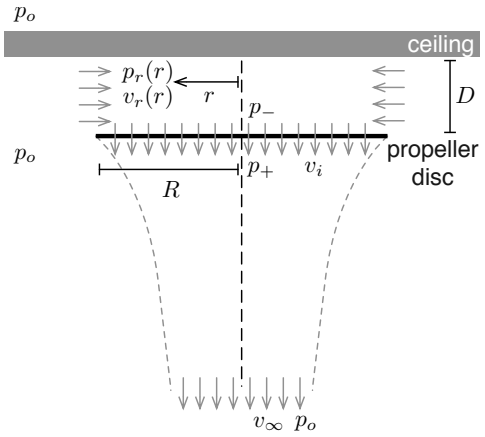

Fig. 2. An axisymmetric propeller disc accelerating the air below a ceiling downwards. The figure shows the fluid pressure and velocity at each section. Just below the ceiling, the pressure and velocity depend on the distance r from the propeller axis.

This lets us evaluate the thrust and torque coefficients of the propeller. These coefficients, typically required for flight control, become functions of the ceiling coefficients. The benchtop experiments were performed to validate the proposed models, accompanied by the analysis of the results. Lastly, we provide some discussion on possible directions of future work.

II. Blade Element Momentum Theory for Ceiling Effects

In this section, we present models for describing the aerodynamic forces and power associated with a spinning propeller in the proximity of a flat surface placed above the rotor. First, a model is developed based on the momentum theory with some simplifying assumptions. Later, the blade element theory is employed to describe the relationship between the rotational rate of the propeller, the generated thrust, and the aerodynamic power.

A. Momentum theory

Consider a spinning rotor of radius R located at the distance D directly below a ceiling as shown in figure 2. We employ standard assumptions: modeling the rotor as an infinitely thin disc, neglecting the boundary layer effects and friction, and assuming the quasi-steady one-dimensional, incompressible flow. For a stationary rotor, such as that of a quadrotor in hover, the rotating propeller induces the constant airflow along the rotating axis at the induced velocity v_i, creating an abrupt change in pressure across the propeller disc. The difference between the downstream (p_+) and upstream (p_-) pressures results in the thrust $T = (p_+ - p_-)\,A$, where $A = \pi R^2$ is the area of the propeller disk. The aerodynamic power is given by $P_a = Tv_i$.

Since the propeller is situated below the ceiling, the upstream air must enter sideways. For a small distance D, it is reasonable to assume that the incoming air travels horizontally and its speed, v_r, is uniform regardless of the distance from the ceiling. This v_r, nevertheless, depends on the distance to the propeller axis. Let r denote the horizontal distance from the propelling axis, then the flow rate of the air entering the region above the propeller is $2\pi rD \cdot v_r(r)$. The fact that the horizontal incoming airflow must vertically exit the region through the propeller yields

$$2\pi rD \cdot v_r(r) = \pi r^2 v_i \quad \text{for } r \in [0, R]$$
$$v_r(r) = \frac{r}{2D} v_i. \tag{1}$$

In addition, the Bernoulli equation allows us to determine the pressure of the air near the ceiling, $p_r(r)$, in comparison to the still air at atmospheric pressure, p_o, infinitely far away, and the pressure immediately above the propeller disc as:

$$p_o = p_r(r) + \frac{1}{2}\rho v_r^2(r) = p_- + \frac{1}{2}\rho v_i^2, \tag{2}$$

where ρ is the air density. Similarly, the downstream pressure and flow velocity satisfy

$$p_+ + \frac{1}{2}\rho v_i^2 = p_o + \frac{1}{2}\rho v_\infty^2, \tag{3}$$

where v_∞ is the terminal velocity of the downstream flow. Traditionally, the momentum theory states that the thrust force T is equal to the difference between the vertical momentum of the incoming and outgoing airflow. However, the presence of the ceiling warrants an additional consideration. The pressure difference between the upper and lower ceiling surface contributes to the vertical momentum of the airflow. That is,

$$T = \dot{m} v_\infty + \Delta p A, \tag{4}$$
$$= (p_+ - p_-)\,A = \frac{1}{2}\rho A v_\infty^2 \tag{5}$$

where Δp is the pressure difference:

$$\Delta p = p_o - \frac{1}{A}\int_{r=0}^{R} p_r(r)\, 2\pi r \mathrm{d}r$$
$$= p_o - \frac{1}{A}\int_{r=0}^{R}\left(p_o - \frac{1}{2}\rho v_r^2(r)\right) 2\pi r \mathrm{d}r \tag{6}$$

and the mass flow rate $\dot{m}$, can be found as the flow across the propeller disc $\dot{m} = \rho A v_i$. Solving equations (1), (4), and (6) leads to

$$\frac{1}{2}\rho A v_\infty^2 - \rho A v_i v_\infty - \frac{1}{16}\rho A v_i^2 \left(\frac{R}{D}\right)^2 = 0. \tag{7}$$

Defining $\delta \coloneqq R/D$ as a propeller-to-ceiling ratio, we obtain one physically feasible solution

$$v_i = \frac{2}{1 + \sqrt{1 + \frac{1}{8}\delta^2}} \frac{1}{2} v_\infty = \frac{1}{2}\gamma^{-1} v_\infty. \tag{8}$$

Here, we have introduced a ceiling coefficient $\gamma \coloneqq \frac{1}{2} + \frac{1}{2}\sqrt{1 + \frac{1}{8}\delta^2}$ to capture the effects of the ceiling. In the absence of ceiling ($\delta \to 0$), $\gamma \to 1$ and $v_i = \frac{1}{2}v_\infty$ as found in regular cases [17]. On the other hand, as the propeller approaches the ceiling, $\delta \to \infty$, and $\gamma \to \infty$.

In fact, we later find in Section IV that the values of γ from the experiments are consistently larger than the

predictions above. To reconcile the discrepancy, we introduce a correction factor α (with a nominal value of 1) to the definition of the ceiling coefficient as

$$\gamma(\delta, \alpha) \coloneqq \frac{1}{2} + \frac{1}{2}\sqrt{1 + \frac{\alpha}{8}\delta^2}. \tag{9}$$

The inclusion of α does not affect γ when $\delta = 0$. This correction factor accounts for several simplifying approximations we made in the derivation, such as the boundary layer effects or the assumptions regarding the uniformity or the direction of airflow leading to equations (6) and (8). In addition, it may include the effective radius of the propeller disc as this correction factor can be absorbed into the definition of δ.

Using the fact that $T = \frac{1}{2}\rho A v_\infty^2$, $P_a = T v_i$ and $v_i = \frac{1}{2}\gamma^{-1} v_\infty$ allows us to relate P_a and T as

$$P_a = \gamma^{-1} T \sqrt{\frac{T}{2\rho A}}. \tag{10}$$

Equation (10) implies that, with the ceiling present ($\gamma > 1$), the propeller requires a factor of γ less power to generate the same thrust.

B. Figure of merit

Thus far, the presented derivation refers to the aerodynamic power P_a as the power delivered by the spinning propeller to the air. In practice, the mechanical power P_m applied to the rotor includes losses from wake rotation, non-uniform flow, and tip vortices not captured by the momentum theory [14], [17]. Small rotors are generally less efficient. The figure of merit, η, accounts for the difference, representing the efficiency of the rotor such that $P_a = \eta P_m$. This figure of merit is typically assumed constant for a particular propeller, regardless of the rotational rate.

C. Blade element theory

The momentum theory provides the relationship between the generated thrust and aerodynamic power. The blade element method considers the geometry of the propeller to estimate the thrust, torque and power when a propeller spins at the rate Ω using the classical airfoil theory. With some algebraic manipulation, we express the result derived in [17] for a fixed-pitch propeller as

$$T = \frac{1}{2}\rho A R^2 \frac{c_1}{c_2}(c_1 - \frac{v_i}{\Omega R})\Omega^2, \tag{11}$$

where we have assumed no horizontal airflow through the propeller. The coefficients c_1 and c_2 are dimensionless quantities related to the pitch angle of the blade, the chord profile, and the number of blades.

D. Blade element momentum theory

By equating the thrust equations from the momentum theory (4) and blade element theory (11), we relate the induced air velocity to the rotational velocity of the propeller as

$$T = \frac{1}{2}\rho A R^2 \frac{c_1}{c_2}(c_1 - \frac{v_i}{\Omega R})\Omega^2 = 2\rho A \gamma^2 v_i^2. \tag{12}$$

It follows the relationship between Ω and v_i can be found from solving the quadratic equation above as

$$\frac{\Omega R}{v_i} = \frac{1}{2c_1}\left(1 + \sqrt{1 + 16 c_2 \gamma^2}\right). \tag{13}$$

This provides us the direct connection between T and Ω as

$$T = \underbrace{2\rho A \left(\frac{2c_1 R\gamma}{1 + \sqrt{1 + 16c_2\gamma^2}}\right)^2}_{c_T} \Omega^2. \tag{14}$$

The conventional thrust coefficient $c_T \coloneqq T/\Omega^2$ is, therefore, dependent on the distance to the ceiling. Without the ceiling, $c_T(\gamma = 1) = 2\rho A\left[2c_1 R/\left(1 + \sqrt{1 + 16c_2}\right)\right]^2$, whereas near the ceiling, $c_T(\gamma \to \infty)$ asymptotically approaches $2\rho A\left[c_1 R/\left(2c_2^{1/2}\right)\right]^2$. To obtain a propeller torque coefficient $c_\tau \coloneqq \tau/\Omega^2$, we consider the aerodynamic power $P_a = T v_i = 2\rho A \gamma^2 v_i^3$ and the fact that the mechanical power is $P_m = \tau\Omega = c_\tau \omega^3$. As a result,

$$P_a = 2\rho A \left(\frac{2c_1 R\gamma^{2/3}}{1 + \sqrt{1 + 16c_2\gamma^2}}\right)^3 \Omega^3 = \eta P_m,$$

$$c_\tau = \frac{P_a}{\eta\Omega^3} = \frac{2\rho A}{\eta}\left(\frac{2c_1 R\gamma^{2/3}}{1 + \sqrt{1 + 16c_2\gamma^2}}\right)^3. \tag{15}$$

III. Benchtop Experiments and Results

In this section, we set up the experiment to verify i.) the relationship between power and thrust depends on the distance between the propeller and ceiling as modeled by equation (10), and ii.) that the thrust and torque coefficients are functions of the ceiling coefficient as given by equations (14)-(15).

A. Experimental setup

We employed 7×16-mm coreless DC motors and propellers with a 23-mm radius ($R = 23$ mm) commercially available as parts for Crazyflie 2.0 for the experiment. A pair of motors and propellers with the opposite spinning directions (to reduce the vibration and measurement noises) are mounted on a force sensor (nano17, ATI) for thrust force measurements, separated by sufficient distance to reduce possible multi-rotor interactions as observed in [16]. A 5 mm-thick transparent acrylic plate was mounted on a linear positioning stage as a ceiling. This allows us to adjust the distance from the propeller to the ceiling with the precision of 20 μm. The experimental setup is illustrated in figure 3.

A computer running a Simulink Real-Time (Mathworks) system with a DAQ (PCI-6229, National Instruments) was used to generate command signals and record the measurements. The driving commands were transmitted to an amplifying circuit for driving both motors. Current sensors (INA169, Texas Instruments) were incorporated to measure the current in the range of $0 - 5$ A with the errors of 2%. The Advent Optical A2108 tachometer with an analog output was installed above the transparent acrylic plate, providing

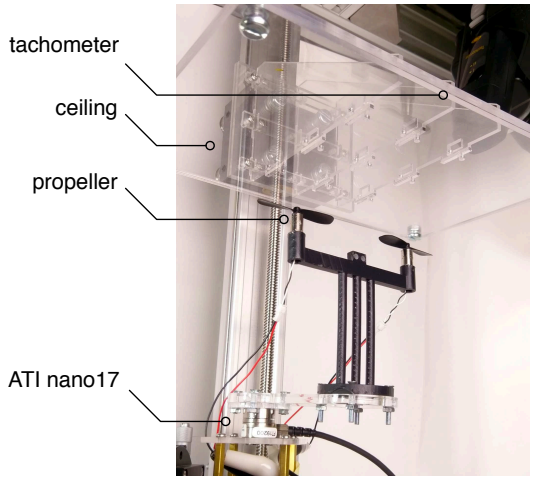

Fig. 3. A photo demonstrating the experimental setup. Two propellers mounted on a force sensor are placed below a flat surface to investigate the ceiling effects.

the rotational rate of the propellers with the uncertainty of $\approx 0.5\%$ or ≈ 10 rad·s^{-1}. The measurements of current and the rotational rate were recorded and synced with the force data via the DAQ at the rate of 5 kHz.

We carried out the measurements with no ceiling present, and at various ceiling distances, from 1.0 mm to 5.0 mm at the increment of 0.5 mm. At each distance, four commanded voltages were tested (2.0, 2.5, 3.0, and 3.5 V). At least ten tests were repeated for each voltage. In each test, we collected the measurements of force, current, and rotational speed. In total, we recorded over 600 data points. All data present are from the averages over two seconds and normalized for a single propeller.

B. Measurement results

The measurements of thrust force, current, and angular velocities are shown in figure 4. It can be seen that, as the voltage increases, the thrust grows as anticipated. At a particular voltage, we observe a radical rise in the thrust force in the presence of the ceiling. For instance, at the input voltage 3.0 V, the averaged thrust measurements were 0.12 N without the ceiling, 0.17 N when the ceiling was 5.0 mm away, and 0.30 N when the ceiling was 1.0 mm away. The enhancement in lift of approximately 2.5 fold when the ceiling was 1.0 mm from the propellers was consistent across all voltages.

The current measurements, nevertheless, were minimally affected by the presence of the ceiling. We found the increase of less than 10% at each voltage across all ceiling distances. This suggests that introduction of the ceiling does not significantly impact the power consumption of the motors. The measurements of the rotational rate also reveal the changes of less than 10% with the ceiling present.

IV. Power, Thrust, and Ceiling Coefficient

A. Mechanical Power

To obtain the mechanical power of the rotor that does not include the losses in the electrical circuit, we consider the first-order motor model in steady state: $V_i = iR_i + V_e$, where V_i is the driving voltage, R_i is the motor's internal resistance, and $V_e = k\Omega$ is the back EMF, linearly proportional to Ω. Using all the measurements of V_i, i, Ω, we solve for R_i and k via the linear least-squares method. Subsequently, the mechanical power can be computed for each measurement as $P_m = iV_e = ik\Omega$. Figure 5A illustrates a plot of the thrust force against the mechanical power at different δ's. The result verifies that the change in ceiling distance has little effect on the power.

B. Figure of merit

The mechanical power computed from the current and voltage measurements can be related to the aerodynamic power and, therefore, thrust force according to equation (10) with the figure of merit defined in section II-B. To evaluate η, we use the fact that $T\sqrt{T/2\rho A} = \eta\gamma P_m$. Figure 5B shows that the plots between P_m and $T\sqrt{T/2\rho A}$ follow the predicted linear trend. Here, only some representative distances are shown to improve the clarity. We then calculated η from the gradient of the best fit line corresponding to the no-ceiling case ($\delta = 0, \gamma = 1$) as $\eta = 0.48$. Since η was evaluated from the measurements without a ceiling only, its value is unaffected by the ceiling effect.

C. Ceiling coefficient and correction factor

To compute the ceiling coefficients from the experimental data, we assume that the figure of merit remains constant, unaffected by the presence of the ceiling. With the value of η previously determined, we evaluate γ's from the gradient of the best fit lines from figure 5B. The values of γ found are plotted as a function of δ as shown as points in figure 5C. It can be seen that the presence of the ceiling boosts the values of γ from unity to $\sim 2 - 3.5$, implying the amplification of thrust by a factor of $\sim 2^{2/3} - 3^{2/3}$ or $\sim 1.6 - 2.3$ for the same power consumption, consistent with the observations in figure 4. This can also be interpreted as the reduction in the input power by a factor $\sim 2 - 3.5$ for the same amount of propelling thrust.

We numerically found that using the correction factor $\alpha = 2.0$ renders the model in good agreement with the experimental data. The model prediction is shown as a dashed line in figure 5C. Slight deviations from the model are seen at larger δ. We omit the data points at $\delta > 15$ (or $D \leq 1$ mm) from the plot as the propeller could have intermittently been in contact with the ceiling from vibration or the system could be in a different flow regime uncaptured by the proposed model.

V. Thrust and Torque Coefficients for Flight

A. Thrust and torque coefficients from the experiments

The measurements of thrust, power, and angular velocity enable us to determine thrust and torque coefficients of the propeller as $c_T := \frac{T}{\Omega^2}$ and $c_\tau := \frac{P_a}{\eta\Omega^3}$. Without a ceiling, these coefficients are constant and only functions of the

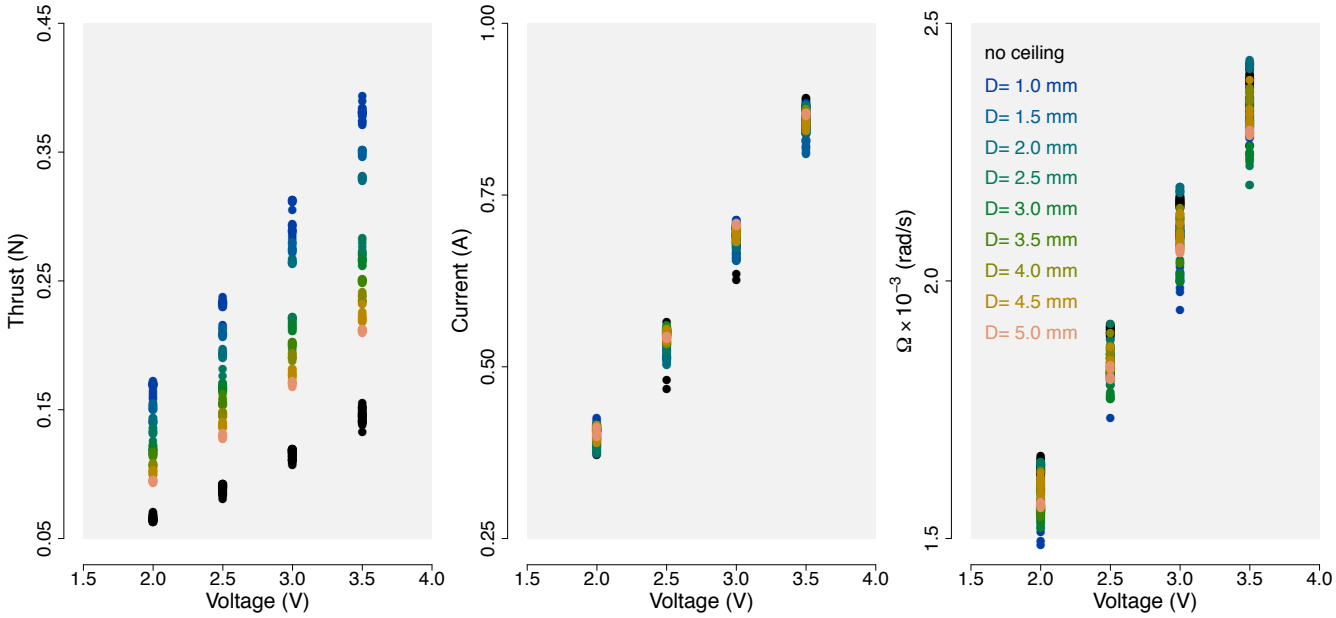

Fig. 4. Measurements of thrust force, current consumption, and the rotational speed of the propeller at different voltage inputs. The displayed values are normalized for one propeller.

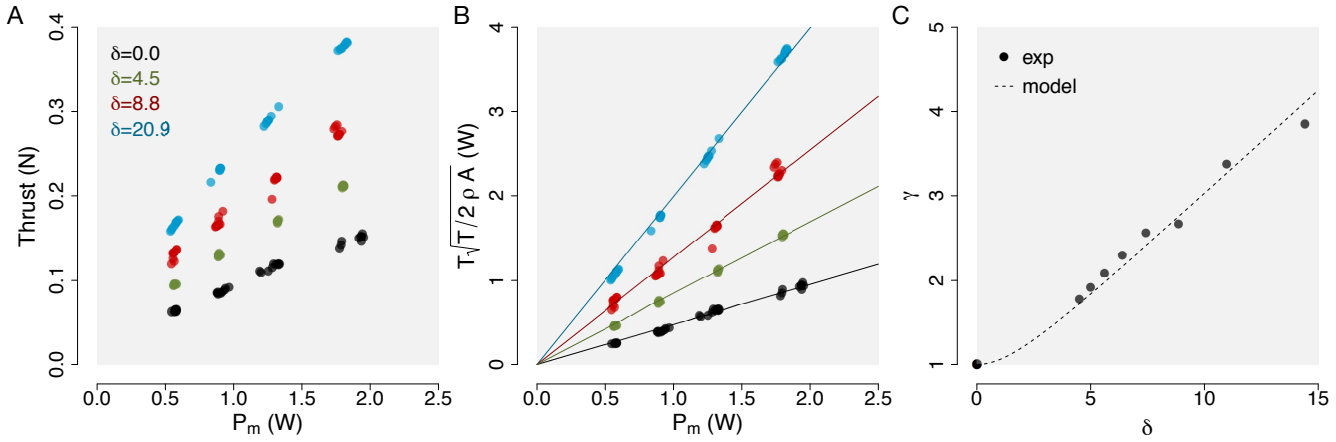

Fig. 5. (A) The plot of mechanical power against the thrust force. (B) The relationship between P_m and $T\sqrt{T/2\rho A}$ is linear as predicted. (C) The ceiling coefficients deduced from the experimental data at different propeller-to-ceiling ratios follows the trend predicted by the model with the correction factor $\alpha = 2.0$.

propeller profile. Without precise knowledge of the blade profile, c_T and c_τ are typically experimentally determined for flight control purposes. With a ceiling in proximity, the BEMT analysis suggests that these coefficients also depend on γ. For each δ, we performed the linear fitting to the equations $T = c_T\Omega^2$ and $P_a = \eta c_\tau \Omega^3$ to calculate c_T and c_τ from the experimental data. The results are illustrated as data points in figure 6.

B. Fitted models for thrust and torque coefficients

The analytical expression of c_T and c_τ depends on γ and the dimensionless parameters; c_1 and c_2, according to the BEMT as provided by equations (14) and (15). Since it is not practical to calculate these parameters for propellers with complicated profiles, we numerically determine the values of c_1 and c_2 that best fit our experimental data for both c_T and c_τ for all δ's. They are found to be 0.157 and 0.160 respectively. Based on these values, we display the model predictions of c_T and c_τ as dashed lines in figure 6.

Overall, the fitted models are in accordance with the experimental data for all γ's. For the thrust coefficient, the model correctly predicts the magnification of up to ~ 2.5 times when the ceiling is 1.5 mm ($\delta \approx 15$) away from the propeller. At the first glance, the discrepancy between the predictions of c_τ and the data seems substantial. A closer inspection, however, reveals that the model accurately predicts minor changes in c_τ, on the order of 20% compared to the no ceiling case. The differences between the model predictions and the data are, in fact, $\approx 10\%$ or less for all ceiling coefficients.

The findings on c_T here are consistent with our initial measurements from figure 4. That is, it explains the marked

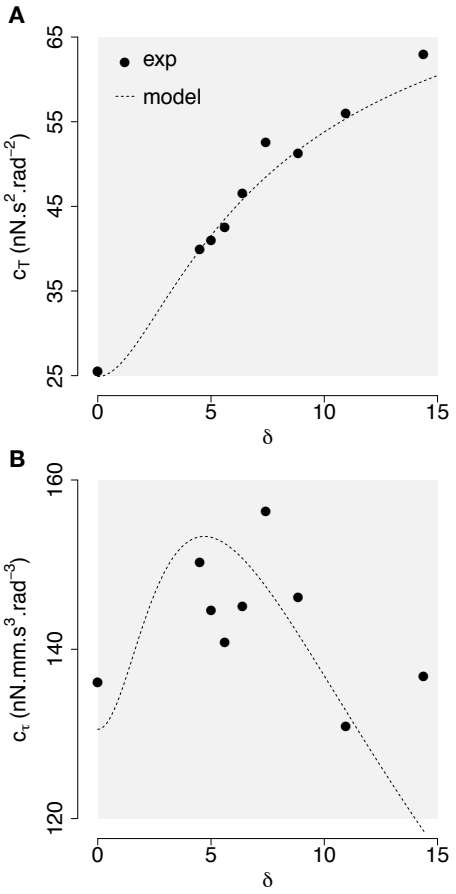

Fig. 6. (A) The thrust coefficient at different distance ratios deduced from the measured thrust and propeller speed (points) and predicted by the model (dashed line). (B) The torque coefficient as calculated from the mechanical power and propeller speed (points) and as predicted by the model (dashed line).

increase in the thrust force and only a slight variation in the rotational speed of the propeller when the ceiling was introduced. The small change in c_τ implies that the propeller consumes, more or less, constant power regardless of the ceiling distance. In total, the ceiling effect contributes to a substantial improvement in thrust, without a noticeable change in the power consumption.

VI. Discussion and Future Work

Based on a few simplifying assumptions, we employed the momentum theory and the blade element method to derive analytical models that capture the effects of a ceiling in the proximity of a spinning propeller. Benchtop experiments were performed and the results obtained are consistent with our model predictions.

We found that the ceiling can reduce the power consumption of a spinning propeller by a factor of three while producing the same thrust. We believe our finding here offers an opportunity to address the issue of diminished flight endurance of small aerial robots. Recently, a number of flying robots employ surface locomotion—perching on vertical surfaces or overhangs—as a strategy to conserve energy and maintain a high vantage point for an extended time [3], [9]. We perceive that a simple modification to the robot as shown in figure 1 would allow a small quadrotor to exploit the ceiling effects for perching on an overhang to prolong the operational time. Based on our results, the approach has potential to increase the flight endurance by a factor of three, without the need for an extra actuator or sophisticated mechanism that may adversely reduce the flight time. To realize such strategy, we are required to further study possible aerodynamic interactions between multiple propellers [16] and other factors such as control and thrust regulating methods that may affect the resultant power efficiency in real flight tests.

References

[1] D. Floreano and R. J. Wood, "Science, technology and the future of small autonomous drones," *Nature*, vol. 521, no. 7553, pp. 460–466, 2015.

[2] P. Chirarattananon, K. Y. Ma, and R. J. Wood, "Perching with a robotic insect using adaptive tracking control and iterative learning control," *The International Journal of Robotics Research*, vol. 35, no. 10, pp. 1185–1206, 2016.

[3] M. Graule, P. Chirarattananon, S. Fuller, N. Jafferis, K. Ma, M. Spenko, R. Kornbluh, and R. Wood, "Perching and takeoff of a robotic insect on overhangs using switchable electrostatic adhesion," *Science*, vol. 352, no. 6288, pp. 978–982, 2016.

[4] L. Daler, S. Mintchev, C. Stefanini, and D. Floreano, "A bioinspired multi-modal flying and walking robot," *Bioinspiration & biomimetics*, vol. 10, no. 1, p. 016005, 2015.

[5] A. Beck, V. Zaitsev, U. B. Hanan, G. Kosa, A. Ayali, and A. Weiss, "Jump stabilization and landing control by wing-spreading of a locust-inspired jumper," *Bioinspiration & biomimetics*, vol. 12, no. 6, p. 066006, 2017.

[6] Y. Mulgaonkar, A. Makineni, L. Guerrero-Bonilla, and V. Kumar, "Robust aerial robot swarms without collision avoidance," *IEEE Robotics and Automation Letters*, vol. 3, no. 1, pp. 596–603, 2018.

[7] J. A. Preiss, W. Honig, G. S. Sukhatme, and N. Ayanian, "Crazyswarm: A large nano-quadcopter swarm," in *Robotics and Automation (ICRA), 2017 IEEE International Conference on*, pp. 3299–3304, IEEE, 2017.

[8] A. Kalantari, K. Mahajan, D. Ruffatto, and M. Spenko, "Autonomous perching and take-off on vertical walls for a quadrotor micro air vehicle," in *Robotics and Automation (ICRA), 2015 IEEE International Conference on*, pp. 4669–4674, IEEE, 2015.

[9] W. R. Roderick, M. R. Cutkosky, and D. Lentink, "Touchdown to take-off: at the interface of flight and surface locomotion," *Interface Focus*, vol. 7, no. 1, p. 20160094, 2017.

[10] M. T. Pope, C. W. Kimes, H. Jiang, E. W. Hawkes, M. A. Estrada, C. F. Kerst, W. R. Roderick, A. K. Han, D. L. Christensen, and M. R. Cutkosky, "A multimodal robot for perching and climbing on vertical outdoor surfaces," *IEEE Transactions on Robotics*, vol. 33, no. 1, pp. 38–48, 2017.

[11] A. Braithwaite, T. Alhinai, M. Haas-Heger, E. McFarlane, and M. Kovač, "Tensile web construction and perching with nano aerial vehicles," in *Robotics Research*, pp. 71–88, Springer, 2018.

[12] A. Betz, "The ground effect on lifting propellers," 1937.

[13] D. A. Griffiths, S. Ananthan, and J. G. Leishman, "Predictions of rotor performance in ground effect using a free-vortex wake model," *Journal of the American Helicopter Society*, vol. 50, no. 4, pp. 302–314, 2005.

[14] G. J. Leishman, *Principles of helicopter aerodynamics with CD extra*. Cambridge university press, 2006.

[15] C. Powers, D. Mellinger, A. Kushleyev, B. Kothmann, and V. Kumar, "Influence of aerodynamics and proximity effects in quadrotor flight," in *Experimental robotics*, pp. 289–302, Springer, 2013.

[16] S. A. Conyers, M. J. Rutherford, and K. P. Valavanis, "An empirical evaluation of ground effect for small-scale rotorcraft," in *Robotics and Automation (ICRA), 2018 IEEE International Conference on*, pp. 1244–1250, IEEE, 2018.

[17] M. Bangura, M. Melega, R. Naldi, and R. Mahony, "Aerodynamics of rotor blades for quadrotors," *arXiv preprint arXiv:1601.00733*, 2016.